

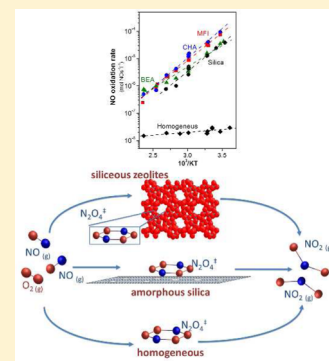
# Catalysis by Confinement: Enthalpic Stabilization of NO Oxidation Transition States by Microporous and Mesoporous Siliceous Materials

Nancy Artioli,<sup>†</sup> Raul F. Lobo,<sup>‡</sup> and Enrique Iglesia\*

Department of Chemical and Biomolecular Engineering, University of California at Berkeley, Berkeley, California 94720-1462, United States

## Supporting Information

**ABSTRACT:** Mesoporous silica and purely siliceous zeolites with voids of molecular dimensions (MFI, CHA, BEA) catalyze NO oxidation by O<sub>2</sub> at near ambient temperatures (263–473 K) with reaction orders in NO and O<sub>2</sub> identical to those for homogeneous routes and with negative apparent activation energies. These findings reflect the stabilization of termolecular transition states by physisorption on surfaces or by confinement within voids in processes mediated by van der Waals forces and without the involvement of specific binding sites. Such interactions lead to the enthalpic stabilization of transition states relative to the gaseous reactants; such enthalpic benefits compensate concomitant entropy losses upon confinement because of the preeminent role of enthalpy in Gibbs free energies at low temperatures. These data and their mechanistic interpretation provide clear evidence for the mediation of molecular transformations by confinement without specific chemical binding at active sites.



## 1. INTRODUCTION

The homogeneous oxidation of nitric oxide (NO) to nitrogen dioxide (NO<sub>2</sub>) with O<sub>2</sub> as the oxidant has been implicated in stratospheric O<sub>3</sub> depletion<sup>1</sup> and in photochemical smog and acid rain in the troposphere.<sup>2</sup> Bodenstein and Wackenheim<sup>3</sup> first showed that reaction rates are proportional to O<sub>2</sub> pressure and second order in NO pressure. This kinetic dependence reflects the stoichiometry of this reaction and was confirmed by later studies<sup>2,4</sup> over a broader range of NO pressure (10<sup>-6</sup> to 1 bar) and temperature (140–650 K).<sup>5</sup> These findings suggest the involvement of a prototypical termolecular transition state with significant entropic barriers, but a more precise mechanistic consensus about the reactive species involved and the connectivity of the atoms in the termolecular transition state has remained elusive.<sup>6</sup> NO oxidation is highly exothermic ( $\Delta H^\circ = -114 \text{ kJ mol}^{-1}$ )<sup>1</sup> and exhibits small and negative apparent activation energies ( $\sim -4 \text{ kJ mol}^{-1}$ );<sup>2,5,6</sup> only the entropic barriers — and the concomitantly small pre-exponential factors — prevent NO oxidation from occurring rapidly at ambient temperatures.

NO oxidation is an enabling chemical transformation in selective catalytic NO<sub>x</sub> reduction (SCR) by NH<sub>3</sub> on metal-exchanged zeolites<sup>7–11</sup> and in NO<sub>x</sub> storage-reduction (NSR) systems.<sup>12,13</sup> Microporous solids, even without active metals or protons, catalyze NO oxidation below ambient temperature.<sup>14</sup> Pentasil (MFI) zeolites containing acid sites (ZSM-5, Si/Al $\sim$ 18)<sup>15</sup> catalyze these reactions to near complete conversion at ambient temperatures, but rates decrease sharply with increasing temperature; such remarkable reactivity and the negative apparent activation energies observed remain un-

explained in mechanistic terms at this time. Similar NO oxidation rates (per mass) were reported on MFI zeolites with different acid site densities (Si/Al = 18–180). Taken together with the observed catalytic effectiveness of NH<sub>4</sub>-exchanged MOR,<sup>16</sup> these data suggest that neither acid sites nor the specific structures of MFI voids are essential for NO oxidation catalysis. Infrared spectra show several adsorbed species (NO<sub>2</sub>, N<sub>2</sub>O<sub>4</sub>, NO<sup>+</sup>, NO<sub>3</sub><sup>-</sup>, and N<sub>2</sub>O<sub>3</sub>) during contact of NO and O<sub>2</sub> on H-MFI, Cu-MFI, CuH-MFI, Na-Y, and Ba-Y,<sup>12b,17</sup> but without concurrent measurements of the reactivity of these materials at relevant catalytic temperatures. Such species, formed via interactions of NO, NO<sub>2</sub> and O<sub>2</sub> with protons or exchanged cations, do not appear to be required for NO oxidation catalysis, which occurs readily on purely siliceous microporous and mesoporous solids.

These high NO oxidation rates on microporous (alumino)-silicates at ambient temperatures stand in sharp contrast with the much higher temperatures required on supported metals ( $\sim 500 \text{ K}$ )<sup>15</sup> and seem to warrant a more precise mechanistic interpretation. Here, we examine the kinetic effects of reactant concentrations and the NO oxidation activation barriers on amorphous mesoporous silica and on microporous purely siliceous forms of pentasil (MFI), beta (BEA), and chabazite (CHA) zeolites. These data confirm the remarkable reactivity of microporous siliceous frameworks, even in the absence of specific sites for chemical binding. These findings, taken

Received: June 26, 2013

Revised: August 19, 2013

Published: September 26, 2013

together with the measured negative activation barriers, lead us to conclude that reactivity is induced by mere physical confinement through van der Waals forces, which provide significant enthalpic stabilization for the relevant termolecular transition states. In doing so, this study provides compelling evidence for the preeminent influence of enthalpy over that of entropy in transition state stabilization at low temperatures, as well as one of the clearest practical manifestations of what has been described in colloquial terms as physical catalysis.<sup>18</sup>

## 2. EXPERIMENTAL METHODS

**2.1. Synthesis and Characterization.** MFI (silicalite-1, SIL-1) was prepared using the fluoride method.<sup>19</sup> Synthesis gels with molar ratios of 1 SiO<sub>2</sub>/0.1 TPAOH/0.1 HF/33 H<sub>2</sub>O were prepared by mixing fumed silica (Cabosil M5) with an aqueous solution of tetrapropylammonium hydroxide (TPAOH; Alfa Aesar, 40 wt %) for 2 h. Aqueous HF (Alfa Aesar, 48 wt %) was then added and the mixture was stirred for 4 h. The resulting gel (pH ~ 5.5) was placed within Teflon-lined stainless steel autoclave (Parr; 23 cm<sup>3</sup>) and kept at 448 K under autogenous pressure for 14 days without stirring. After cooling to ambient temperature, the solids were recovered by filtration, washed with DI water until the pH of the filtrate was lower than 9, and left overnight in ambient air. The structure-directing agent was removed by heating to 823 K at 0.05 K s<sup>-1</sup> in ambient air and holding for 6 h.

Silicalite-1 (SIL-1D) with intracrystalline silanols was prepared using OH<sup>-</sup> instead of F<sup>-</sup> as the mineralizing agent.<sup>20</sup> SIL-1D was prepared from a gel of molar composition 40 SiO<sub>2</sub>/9 TPAOH/1500 H<sub>2</sub>O using Ludox-AS40 (Aldrich) as the silica source.<sup>21</sup> This gel was prepared by adding the Ludox suspension to an aqueous solution of TPAOH (40% Alfa Aesar) and stirring for 5 h; this gel (pH > 13) was placed in a Teflon-lined stainless steel autoclave (23 cm<sup>3</sup>; Parr) and kept at 423 K under autogenous pressure for 3 days without stirring. The solids were recovered by filtration, washed with deionized water until the filtrate pH was <9, kept in ambient air overnight, and then treated as in the case of SIL-1, but holding at 878 K for 10 h.

Pure-silica BEA was prepared using 4,4-trimethylene bis-*N*-methyl-*N*-benzylpiperidinium hydroxide (TMP(OH)<sub>2</sub>) as the structure director (SD; prepared using reported procedures<sup>22</sup>), tetraethylorthosilicate (TEOS) as the silica source, and gels of molar composition 1 TEOS/20 H<sub>2</sub>O/0.25 TMP(OH)<sub>2</sub>. All reagents were stirred vigorously within a sealed plastic container until the hydrolysis of TEOS was confirmed by the formation of a clear solution (~3 h). This solution was kept at 393 K for 5 days within a Teflon-lined autoclave (23 cm<sup>3</sup>; Parr) K at its autogenous pressure without stirring. The solids were recovered by centrifugation (200 Hz); the process was repeated with fresh water aliquots until the pH of the supernatant solution was below 9. The organic structure director was removed by heating to 823 K at 0.08 K s<sup>-1</sup> in ambient air and holding for 10 h.

Pure-silica chabazite (CHA) was prepared in fluoride media using reported procedures.<sup>23</sup> Trimethyladamantylammonium hydroxide (Sachem) was used as the structure director, and TEOS as the silica source. The samples were treated in ambient air first by heating to 423 K at 0.17 K s<sup>-1</sup> and holding for 10 h and then by heating at 0.03 K s<sup>-1</sup> to 823 K and holding for 6 h.

Amorphous mesoporous SiO<sub>2</sub> (Selecto, Fisher Scientific, 32–63 μm aggregates) was used to probe the reactivity of silicate surfaces in the absence of microporous confinement.

This sample was treated in flowing He (Praxair, 99.999% purity; 33.3 cm<sup>3</sup> g<sup>-1</sup>·s<sup>-1</sup>) by heating at 0.08 K s<sup>-1</sup> to 773 K and holding for 4 h.

Crystal structures were confirmed by X-ray diffraction (Philips X'pert diffractometer) using a Cu Kα source (5° to 50° 2θ, 0.02° step size, 2 s hold). Textural properties were measured using N<sub>2</sub> adsorption (Micromeritics ASAP 2020) after treatment in vacuum at 573 K for 8 h. Micropore volumes were determined using the *t*-plot method with the Harkins–Jura equation to estimate the statistical thickness *t*.<sup>24,25</sup>

**2.2. NO Oxidation Rates and Mechanism.** NO oxidation rates were measured on powders (125–177 μm, 80–120 mesh) held onto a porous quartz frit within a U-shaped quartz tube (10 mm O.D.). Reactant mixtures (15% O<sub>2</sub>/He, 2% NO/He, Praxair 99.999% purity) and He (Praxair, 99.999% purity) were metered with electronic mass-flow controllers (Porter Instruments) to give the desired O<sub>2</sub> (1–10 kPa) and NO (0.025–0.5 kPa) pressures. Water traps were kept on transfer lines to the reactor in order to avoid H<sub>2</sub>O within the zeolite bed. Temperatures (278–423 K) were measured with a K-type thermocouple and maintained constant by resistive heating using a temperature controller (Watlow, 96 series). Temperatures below ambient levels were kept constant using the gaseous effluent from a liquid N<sub>2</sub> Dewar vessel.

Inlet and outlet concentrations of NO and NO<sub>2</sub> streams were measured with an infrared analyzer (MKS Multi Gas Analyzer 2030, 2 cm<sup>3</sup> cell; 2 cm path length). NO oxidation rates are reported normalized by catalyst surface area (moles NO converted m<sup>-2</sup>·s<sup>-1</sup>), because of the absence of specific sites or heteroatoms in purely siliceous materials. Rates were measured at NO and O<sub>2</sub> conversions below 20% and plug-flow hydrodynamic formalisms were used to correct for small changes in reactant concentrations along the bed and to report rates at inlet conditions even at these low conversions. Rates are also reported on the basis of zeolite micropore volume (see Table 1) defined as the pore space occupied by nitrogen via

**Table 1. Textural Properties of Mesoporous Silica and Pure-Silica Zeolites**

	sample				
	silica	SIL-1	SIL-1D	BEA	CHA
microporous volume, cm <sup>3</sup> g <sup>-1a</sup>		0.14	0.15	0.17	0.27
micropore area, m <sup>2</sup> g <sup>-1</sup>	446	440	440	688	606

<sup>a</sup>Micropore volumes were determined using the *t*-plot method with the Harkins–Jura equation to estimate the statistical thickness *t*.<sup>24,25</sup>

absorption technique. This allows direct comparison of catalytic rates within and outside constrained spaces of subnanometer size. Samples were treated in flowing 5% O<sub>2</sub>/He mixtures (Praxair 99.999% purity, 33.3 cm<sup>3</sup> g<sub>cat</sub><sup>-1</sup>·s<sup>-1</sup>) by heating to 723 K at 0.03 K s<sup>-1</sup> and holding for 4 h to remove traces of adsorbed water and other species before rate measurements.

## 3. RESULTS

### 3.1. Structural Properties of Porous Silicate Materials.

X-ray diffractograms showed that all microporous samples were highly crystalline and did not show detectable crystallographic impurities. Their micropore volumes were consistent with the intended framework structures,<sup>26,21</sup> except for BEA, for which the measured micropore volume (0.17 cm<sup>3</sup> g<sup>-1</sup>) was smaller than theoretical values (0.22–0.24 cm<sup>3</sup> g<sup>-1</sup>).<sup>27,28</sup> There is no apparent reason for this difference, because all characterization

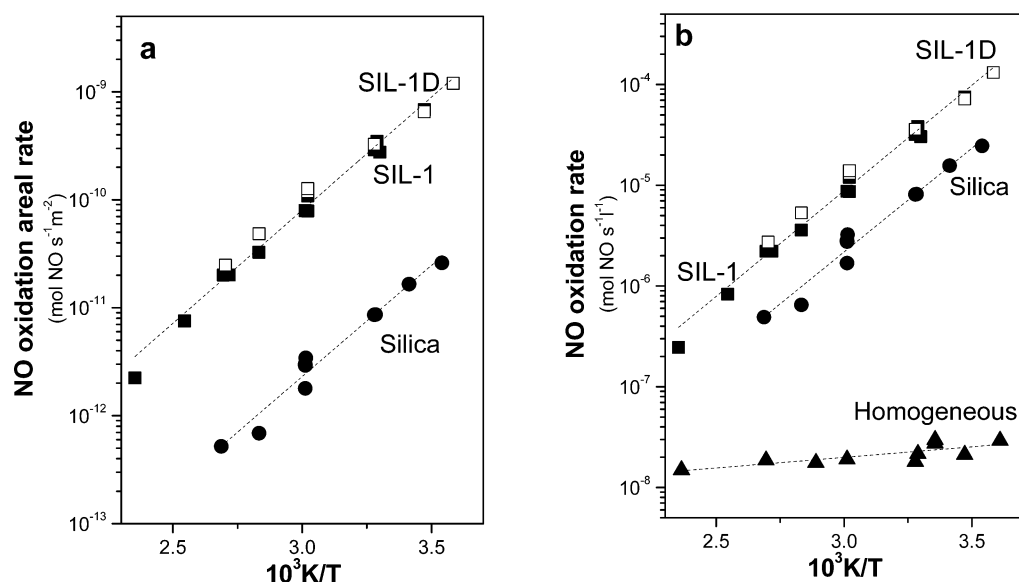


**Figure 1.** (a) Forward NO oxidation areal rates (100 Pa NO, 5 kPa O<sub>2</sub>) on SIL-1 (■), SIL-1D (□), and silica (●). (b) Forward NO oxidation rates (100 Pa NO, 5 kPa O<sub>2</sub>) on SIL-1 (0.1 g) (■), SIL-1D (0.1 g) (□), silica (0.8 g) (●), and empty reactor cell (4.4 cm<sup>3</sup>) (▲).

techniques (XRD, SEM, and UV–vis spectroscopy) indicate that the samples are highly crystalline and lack detectable impurities. In our analysis below, we use the measured micropore volumes of these zeolite samples (Table 1) to quantify specific reaction rates on a volumetric basis. Al was not detected in any of the samples by energy dispersive analysis spectroscopy in a JEOL JSM7400F microscope.

**3.2. NO Oxidation Rates on Microporous and Mesoporous Silicates.** NO oxidation rates were measured as a function of NO and O<sub>2</sub> pressures (50–450 Pa NO, 1–10 kPa O<sub>2</sub>) at 278–435 K on silica, SIL-1, SIL-1D, CHA, and BEA. Measured NO consumption rates ( $r_{\text{NO}}$ ) reflect net reaction rates, given by differences between the rates in the forward and reverse directions for this reaction (NO oxidation ( $r_{\text{NO}}^+$ ) and NO<sub>2</sub> decomposition ( $r_{\text{NO}}^-$ ) rates):



Measured rates are related to the forward rates by the approach to equilibrium parameter ( $\eta$ ) for the stoichiometric reaction depicted in eq 1:

$$r_{\text{NO}} = r_{\text{NO}}^+ - r_{\text{NO}}^- = r_{\text{NO}}^+(1 - \eta) \quad (2)$$

$$\eta = \left( 1 - \frac{[\text{NO}_2]^2}{K_1[\text{NO}]^2[\text{O}_2]} \right) \quad (3)$$

where  $K_1$  is the equilibrium constant for the NO oxidation reaction as written in eq 1 and [NO], [NO<sub>2</sub>], and [O<sub>2</sub>] are the reactant and product concentrations (in units of atm). Forward NO oxidation rates are then given from measured rates by

$$r_{\text{NO}}^+ = \frac{r_{\text{NO}}}{(1 - \eta)} \quad (4)$$

Figure 1a shows forward NO oxidation areal rates on SIL-1 and SIL-1D (100 Pa NO, 5 kPa O<sub>2</sub>, 278–435 K). NO oxidation rates are also reported on a reactor volume basis (Figure 1b) in order to assess any contributions from homogeneous reactions in comparisons between experiments with and without siliceous solids within the reactor.

Silicalite-1 samples prepared in hydroxide media (SIL-1D) typically show high concentrations of defects, such as missing framework atoms and H-bonded silanols.<sup>20</sup> Fluoride synthesis protocols (SIL-1) avoid these defects and the concomitant formation of silanol groups (below detection levels by <sup>29</sup>Si MAS NMR).<sup>29</sup> These differences in silanol densities between SIL-1 and SIL-1D did not lead to different NO oxidation rates (Figure 1), indicating that silanols or other defects do not preferentially catalyze NO oxidation at near ambient temperatures. Areal NO oxidation rates were also measured on amorphous silica (Selecto, surface area 446 m<sup>2</sup>g<sup>-1</sup>) at 100 Pa NO, 5 kPa O<sub>2</sub> and 278–435 K (Figure 1a). Areal rates were 15–50 times smaller on amorphous silica than on SIL-1 in this temperature range (Figure 1a), but much higher than homogeneous rates (Figure 1b). These data indicate that amorphous siliceous surfaces, even without voids of nanometer size, catalyze NO oxidation rates; such surfaces are, however, much less effective than siliceous surfaces within small channels or voids, which appear to solvate the relevant transition states for NO oxidation more effectively than the surfaces of mesopores.

Homogeneous reaction rates were also measured in empty reactors at these conditions (100 Pa NO, 5 kPa O<sub>2</sub>; 278–435 K); these rates are reported in Figure 1b, together with those measured on amorphous SiO<sub>2</sub>, SIL-1D, and SIL-1. All rates in Figure 1b are normalized by the total reactor volume in order to illustrate the catalytic enhancements brought forth by purely siliceous solids (0.1 g for SIL and SIL-1, 0.8 g for silica). Homogeneous NO oxidation rates are much lower than in the presence of SIL-1 and SIL-1D samples at all temperatures (by factors of 20 to 10 000), indicating that microporous solids mediate the pathways responsible for measured NO oxidation rates. These catalytic pathways become increasingly prevalent with decreasing temperature, because their apparent activation energies are much more negative on siliceous solids than for homogeneous routes (Figure 1b). For instance, NO oxidation rates at 278 K on SIL-1D (0.1 g) are 4500 times larger than in empty reactors (4.4 cm<sup>3</sup>), a difference that becomes much smaller (20-fold) at 435 K. These data also confirm that homogeneous contributions to measured rates can be neglected

in the measurement and mechanistic analysis of all catalytic rate data reported here.

The evident catalytic properties of amorphous SiO<sub>2</sub> (Figure 1b) indicate that mere physical adsorption on mesoporous surfaces can significantly increase NO oxidation rates over those for homogeneous routes; the even higher areal rates on SIL provide compelling evidence for the stabilization of the relevant transition states by confinement within voids of nanometer size, even in the absence of specific binding sites. These conclusions are consistent with NO oxidation pathways catalyzed also by other purely siliceous zeolites, such as beta (BEA; three-dimensional 12-ring pore system with 0.74 nm pore diameter)<sup>30</sup> and chabazite (CHA; a three-dimensional pore system with 0.74 × 0.84 nm cages connected via 0.38 nm 8-ring windows)<sup>30</sup> (Figure 2).

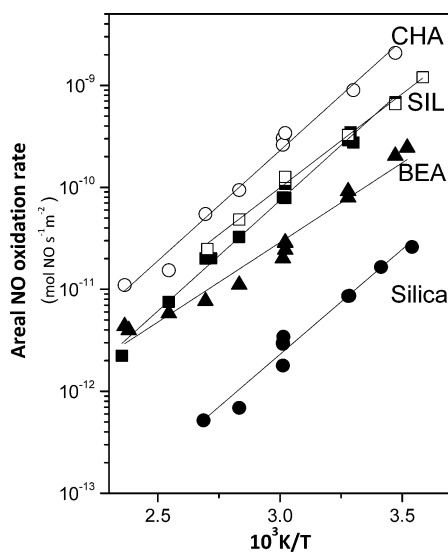
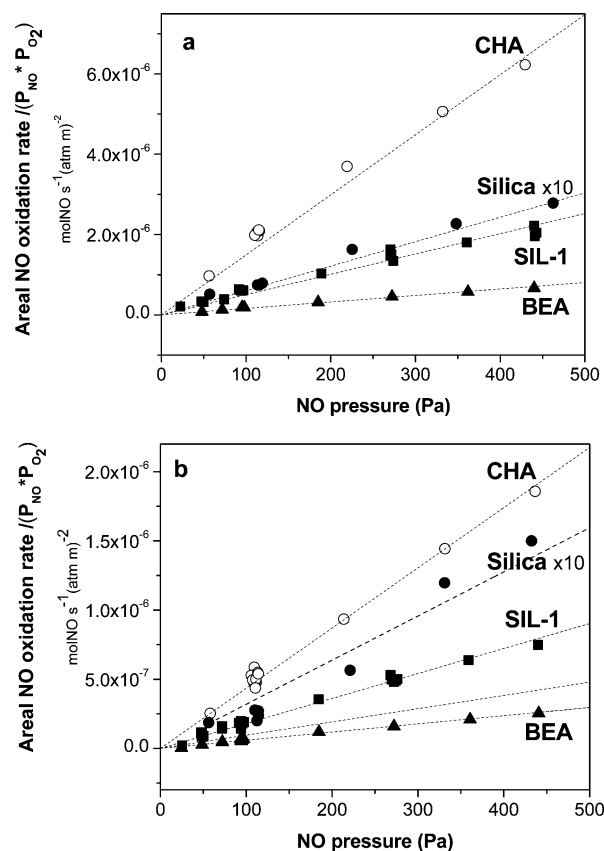


**Figure 2.** Arrhenius plots of forward areal NO oxidation rates (100 Pa NO, 5 kPa O<sub>2</sub>); on SIL-1 (■), SIL-1D (□), BEA (▲), CHA (○), and silica (●).

NO oxidation rates showed similar kinetic dependences on NO and O<sub>2</sub> pressures and similar negative apparent barriers on pure silica BEA, CHA, and SIL (section 3.3). On all zeolites, areal rates were 15–20 times larger than on amorphous silica in the temperature range used (278–435 K). The mechanistic origins of such confinement effects are examined below in the context of the kinetic behavior and reaction pathways for NO oxidation via homogeneous and catalytic routes. Specifically, we address the origins of the negative apparent activation barriers and the molecularity of the relevant transition states within the context of mechanistic routes proposed previously for homogeneous NO oxidation.

**3.3. Effect of NO and O<sub>2</sub> Partial Pressure on NO Oxidation Rates.** NO oxidation rates ( $r_{\text{NO,gas}}^+$ ) were measured as a function of NO pressure (50–450 Pa) at 305 and 331 K on amorphous SiO<sub>2</sub>, SIL-1, BEA, and CHA. These data are reported in Figure 3 as areal NO oxidation rates divided by the NO and O<sub>2</sub> pressures. These data would be accurately described by a single line with zero intercept at all NO and O<sub>2</sub> pressures when NO oxidation rates obey the equation:

$$r_{\text{NO,gas}}^+ = k_1^+ [\text{NO}]^2 [\text{O}_2] \quad (5)$$

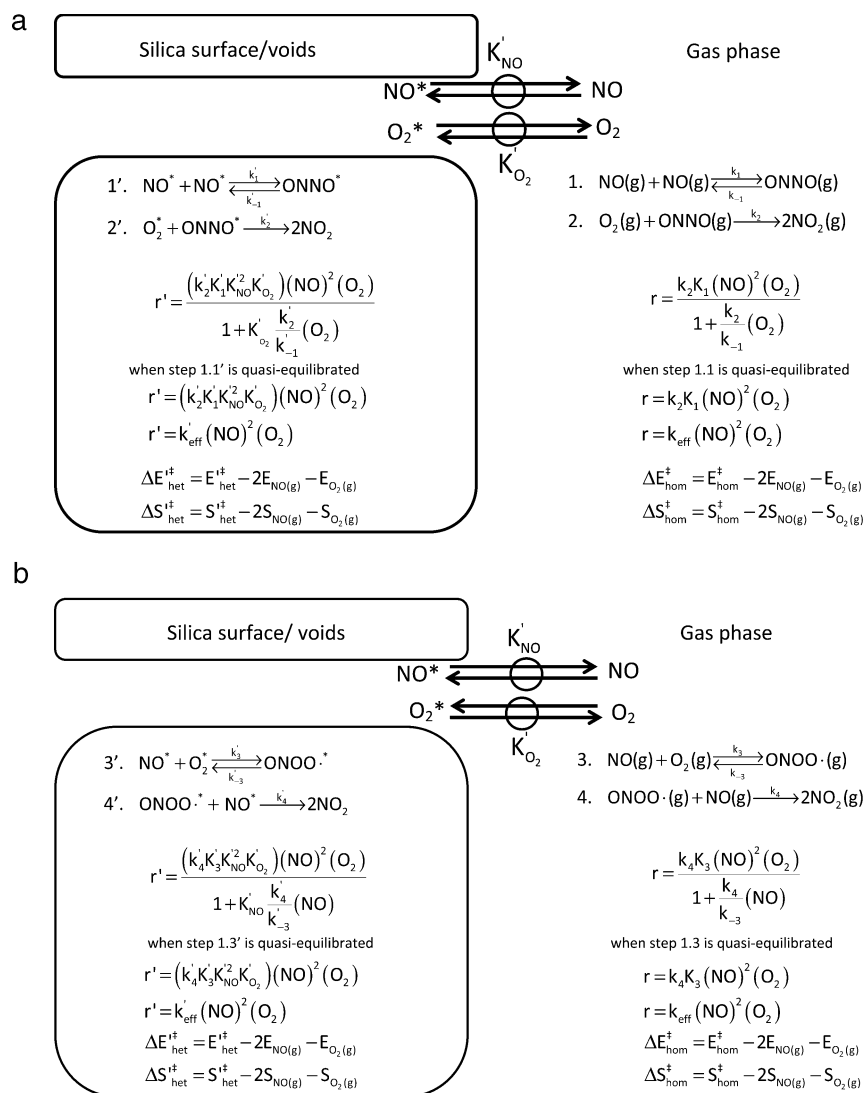


**Figure 3.** Areal NO oxidation (forward) rates divided by NO and O<sub>2</sub> pressures (50–450 Pa NO, 1–10 kPa O<sub>2</sub>) on SIL-1 (0.1 g) (■), BEA (0.1 g) (▲), CHA (0.3 g) (○), and silica (0.8 g) (●) as a function of NO pressure at two temperatures of (a) 305 K and (b) 331 K.

Such an equation has been reported to describe homogeneous rates accurately over a broad range of pressure and temperature.<sup>2,31,32</sup>

All catalytic rate data on SIL-1 (305 K, Figure 3a; 331 K, Figure 3b) were accurately described by the functional form of eq 5, suggesting that catalytic and homogeneous pathways involve kinetically relevant transition states containing two NO molecules and one O<sub>2</sub> molecule. As in the case of any kinetic analysis, the specific connectivity among the atoms in these transition states is neither accessible from the data nor relevant to conclusions about the number and type of atoms at such transition states. These data also suggest that rate enhancements reflect the stabilization of these termolecular transition states by physical confinement (and even physisorption on flat surfaces) through nonspecific van der Waals forces, instead of different elementary steps for catalytic and homogeneous NO oxidation routes.

NO oxidation rates were also measured as a function of O<sub>2</sub> pressure (1–10 kPa) at 100, 270, and 440 Pa NO at 305 K (Figure 3a) and at 100 and 270 Pa NO at 331 K (Figure 3b) on amorphous silica, SIL-1, BEA and CHA. These data are also accurately described by eq 5 as shown by the overlap of all rate data at different NO and O<sub>2</sub> pressures (Figure 3) and show that the NO<sub>2</sub> molecules formed (at different concentrations in these experiments) do not influence *forward* NO oxidation rates. The different slopes among these siliceous materials merely reflect their different reactivity, conferred by confinement effects that strengthen as voids become similar in size to the termolecular transition states that mediate NO oxidation catalysis.

Scheme 1<sup>a</sup>

<sup>a</sup>(a) NO oxidation via NO dimer intermediate and (b) NO oxidation via peroxynitrite radical intermediate in homogeneous and heterogeneous phases.

#### 4. DISCUSSION

In what follows, we discuss plausible mechanistic proposals for the observed NO oxidation rate enhancements induced by siliceous frameworks, especially those with voids of molecular dimensions. In doing so, we preserve the termolecular nature (but not necessarily the specific atomic connectivity within) of the transition states previously proposed to mediate homogeneous routes. We explore the consequences of their confinement via nonspecific dispersion forces as the root cause of the high reactivity and negative apparent activation energies on these porous solids, which reflect enthalpic stabilization of the transition states relative to reactants without large commensurate losses in transition state entropies.

NO oxidation rates on mesoporous and microporous siliceous solids show the same NO and O<sub>2</sub> kinetic dependences as in the homogeneous routes (section 3). These kinetic effects of reactant concentrations and the negative activation energies observed are consistent with the elementary steps in Scheme 1, which describe homogeneous pathways in the right panel and the corresponding steps upon adsorption or confinement of

reactants and transition states in the left panel. Scheme 1a and b differ only in the nature of the intermediates and possibly in the (kinetically inaccessible) specific connectivity among the atoms present in the termolecular transition state. We include both possible routes for completeness and because of their unresolved respective contributions to homogeneous pathways, but the conclusions we reach are unaffected in any way by the specific choice of intermediates.

Scheme 1a shows the reversible formation of NO dimers and their subsequent irreversible reaction with O<sub>2</sub> in a step mediated by a termolecular transition state with the atomic stoichiometry of N<sub>2</sub>O<sub>4</sub>. ONNO dimers have been detected as stable species in liquid and solid forms and also during photolysis of *syn*-N<sub>2</sub>O<sub>4</sub> (in an Ar solid matrix at 6.3 K), where *cis*-(ONNO)·O<sub>2</sub> complexes are detected as the sole reactive intermediate due to the instability of gaseous *trans*-(ONNO)·O<sub>2</sub> complexes at ambient temperatures.<sup>6a</sup>

The right panel shows the rate equation derived from the assumption of pseudo-steady-state for NO dimer intermediates for homogeneous routes:

$$r = \frac{k_2 K_1 (\text{NO})^2 (\text{O}_2)}{1 + \frac{k_2}{k_{-1}} (\text{O}_2)} \quad (6)$$

This equation simplifies to the form of the measured rate equation for homogeneous NO oxidation routes:

$$r = k_2 K_1 (\text{NO})^2 (\text{O}_2) \quad (7)$$

when dimer formation steps are quasi-equilibrated ( $k_2(\text{O}_2) \ll k_{-1}$ ); the contrasting assumption of irreversible NO dimer formation makes NO oxidation rates proportional to  $(\text{NO})^2$  and independent of  $(\text{O}_2)$ , in contradiction with measured rates. The effective rate constant ( $k_{\text{eff}} = k_2 K_1$ ) in eq 7 can be expressed in terms of activation energies and entropies using the formalism of transition state theory:

$$\Delta E_{\text{hom}}^\ddagger = E_{\text{hom}}^\ddagger - 2E_{\text{NO(g)}} - E_{\text{O}_2(\text{g})} \quad (8)$$

$$\Delta S_{\text{hom}}^\ddagger = S_{\text{hom}}^\ddagger - 2S_{\text{NO(g)}} - S_{\text{O}_2(\text{g})} \quad (9)$$

These relations show that thermodynamic properties of the transition state are “measured” relative to the gaseous reactants that form it in the context of the elementary steps in Scheme 1a and the observed rate equation.

The left panel in Scheme 1a considers the initial physisorption (on surfaces) or confinement (within voids) of  $\text{NO}(\text{g})$  and  $\text{O}_2(\text{g})$  within purely siliceous solids (to form  $\text{NO}^*$  and  $\text{O}_2^*$ ) without specific binding sites. Here, the asterisk (\*) represents species interacting within their surrounding environment via nonspecific interactions with a siliceous framework. The form of the measured rate equation implies that adsorbed  $\text{NO}^*$  and  $\text{O}_2^*$  intermediates on surfaces or within zeolite voids are present at concentrations well below saturation levels; in such cases, their concentrations become proportional to the respective pressures of NO and  $\text{O}_2$ , through their respective adsorption constants ( $K'_{\text{NO}}$  and  $K'_{\text{O}_2}$ ). These adsorbed or confined species then react via intermediates and transition states similar in composition to those that mediate homogeneous routes, but whose energies and entropies reflect their respective confinement within small voids. The corresponding rate equations for reversible and quasi-equilibrated dimer formation are

$$r' = \frac{(k'_2 k'_1 k'_{\text{NO}} k'_{\text{O}_2}) (\text{NO})^2 (\text{O}_2)}{1 + K'_{\text{O}_2} \frac{k'_2}{k'_{-1}} (\text{O}_2)} \quad (10)$$

and

$$r' = (k'_2 k'_1 k'_{\text{NO}} k'_{\text{O}_2}) (\text{NO})^2 (\text{O}_2) \quad (11)$$

respectively. The functional form of eq 11 accurately describes all measured NO oxidation rates on SIL-1, BEA, and CHA zeolites and on mesoporous silica. The grouping of kinetic and thermodynamic parameters in eq 11 assigns chemical significance to the rate coefficients, which are given by the slopes of the lines in Figure 3.

The corresponding activation energies and entropies for the effective catalytic rate constant in eq 11 are given by

$$\Delta E'_{\text{het}}^\ddagger = E'_{\text{het}}^\ddagger - 2E_{\text{NO(g)}} - E_{\text{O}_2(\text{g})} \quad (12)$$

$$\Delta S'_{\text{het}}^\ddagger = S'_{\text{het}}^\ddagger - 2S_{\text{NO(g)}} - S_{\text{O}_2(\text{g})} \quad (13)$$

Equations 12 and 13 differ from eqs 8 and 9 only in their respective first terms, which reflect the energy and entropy of a confined transition state measured, as in the case of homogeneous routes, with respect to the gaseous (unconfined) molecules that form the confined termolecular transition state. Catalytic enhancements induced by confinement are defined here as the ratio of catalytic to homogeneous rates. These ratios depend only on the free energy differences (and thus enthalpy and entropy differences) between their respective confined and unconfined transition states. Such differences must reflect, in turn, van der Waals stabilization as well as any differences in the connectivity among the atoms in the transition state conferred by confinement. In either instance, the catalytic consequences arise from nonspecific physical interactions instead of specific binding, thus mediating the formation and cleavage of chemical bonds solely by dispersion forces. We note that the stabilization of the *reactants* and *intermediates* by confinement or adsorption is not relevant to the dynamics of NO oxidation on siliceous solids, because only their gaseous (unconfined) thermodynamic properties appear in eqs 12 or 13. This follows rigorously from the measured kinetic orders in NO and  $\text{O}_2$  without requiring any specific or additional mechanistic assumptions or interpretations.

Scheme 1b depicts another plausible mechanistic proposal. It involves the reversible formation and irreversible decomposition of peroxynitrite radicals ( $\text{ONOO}\cdot$ ). Such radicals have been detected by electron paramagnetic resonance and they are considered to be important intermediate in NO oxidation by  $\text{O}_2$ . The formation of  $\text{ONOO}\cdot$  could be also followed by isomerization to  $\text{NO}_3\cdot$ , but this is unlikely under the condition used in the gas-flow reactor.<sup>33</sup>

The detailed steps and rate equations are included in Scheme 1b and the treatment and equations resemble in functional form and in thermodynamic interpretation those in Scheme 1a. The general rate equation derived from  $\text{ONOO}\cdot$ -mediated routes

$$r' = \frac{(k'_4 k'_3 k'_{\text{NO}} k'_{\text{O}_2}) (\text{NO})^2 (\text{O}_2)}{1 + k'_{\text{NO}} \frac{k'_4}{k'_{-3}} (\text{NO})} \quad (14)$$

differs from that derived for the case of NO dimers as intermediates (eq 10), but its asymptotic form for quasi-equilibrated  $\text{ONOO}\cdot$ -formation (step 3', Scheme 1b):

$$r' = (k'_4 k'_3 k'_{\text{NO}} k'_{\text{O}_2}) (\text{NO})^2 (\text{O}_2) \quad (15)$$

is identical in functional form to eq 11 derived from the elementary steps in Scheme 1. It differs from that for pathways mediated by NO dimers (eq 11) only in the chemical significance of the effective rate constant. We conclude that the specific steps involved and the atomic connectivity in the relevant transition state are neither experimentally discernible nor consequential for our treatment; the NO and  $\text{O}_2$  kinetic effects depend only on the number and type of atoms that compose the transition state and on its concomitant formation from two NO and one  $\text{O}_2$  species in pre-equilibrated steps, all of which follow rigorously from the measured kinetic orders. Neither mechanism (Scheme 1a or b) would describe the measured kinetic dependence of NO oxidation rates when their respective first steps are irreversible and therefore kinetically relevant.

Next, we examine measured rate constants using the formalism of transition state theory. We aim to relate

(N<sub>2</sub>O<sub>4</sub><sup>‡</sup>) transition state concentrations within small voids or at siliceous surfaces to NO and O<sub>2</sub> concentrations in the unconfined gas phase using thermodynamic relations. In doing so, it is necessary and convenient to choose standard states of similar units for gaseous and confined phases (see Appendix in the Supporting Information for details). We choose here 1 mol (*m*<sub>ref</sub><sup>3</sup>)<sup>-1</sup> as the standard state, where the relevant reference volume is taken as entire gaseous phase (*m*<sub>homog</sub><sup>3</sup>) for the homogeneous system and as the micropore volume (*m*<sub>micro</sub><sup>3</sup>) for the zeolites, which rigorously represents the confined reaction space for zeolites (Table 1). On silica mesopores, we define the reactive volume from its surface area by assuming an active layer that mimics that of the relevant termolecular transition state. The latter is taken as the molecular diameter of N<sub>2</sub>O<sub>4</sub> (0.58 nm, from its liquid density<sup>34</sup>) and gives a reactive volume of 0.262 cm<sup>3</sup> g<sup>-1</sup> for the amorphous SiO<sub>2</sub> used in this study. The reference volume is taken as that of this active layer (*m*<sub>layer</sub><sup>3</sup>). This selection of standard states and active volumes allows comparisons of volumetric rates among samples and entropy estimates using consistent units for the standard state, which is essential for our subsequent treatment of kinetic parameters using the formalism of molecular thermodynamics and transition state theory.

Measured rate constants can be expressed for homogeneous and catalytic pathways on a volume basis<sup>35</sup> as a function of the effective Gibbs free energy ( $\Delta G_{\text{eff}}^{\circ}$ ), which defines the effective rate constant:

$$k_{\text{eff}} = 2 \frac{k_{\text{B}}T}{h} \exp\left(-\frac{\Delta G_{\text{eff}}^{\circ}}{RT}\right) \left[\frac{\text{mol}}{m_{\text{ref}}^3}\right] \left[\frac{\text{mol}}{m_{\text{homog}}^3}\right]^{-3} \quad (16)$$

This equation can be expressed in terms of effective enthalpies ( $\Delta H_{\text{eff}}^{\circ}$ ) and entropies ( $\Delta S_{\text{eff}}^{\circ}$ ) of formation of the transition state:

$$k_{\text{eff}} = 2 \frac{k_{\text{B}}T}{h} \exp\left(\frac{\Delta S_{\text{eff}}^{\circ}}{R}\right) \exp\left(-\frac{\Delta H_{\text{eff}}^{\circ}}{RT}\right) \left[\frac{\text{mol}}{m_{\text{ref}}^3}\right] \left[\frac{\text{mol}}{m_{\text{homog}}^3}\right]^{-3} \quad (17)$$

which are determined, in turn, from the temperature dependence of the measured rate constants. These thermodynamic properties reflect only those for transition states and gaseous reactants (from eqs 8 and 9 (or eqs 12 and 13)) and thus depend on the catalyst properties only through the adsorption or confinement of the transition state.  $\Delta H_{\text{eff}}^{\circ}$  and  $\Delta S_{\text{eff}}^{\circ}$  values determined from measured NO oxidation rates (section 3) for mesoporous and microporous silicate catalysts and for the homogeneous reactions are shown in Table 2.

Adsorption (on mesoporous silica) and confinement (within microporous silicates) enhance NO oxidation rates by stabilizing transition states (relative to the same gaseous NO and O<sub>2</sub> reactants as in the homogeneous routes) by the mere act of adsorbing or confining such transition states (eqs 12 and 13). Indeed, activation enthalpies are more negative on mesoporous silica than for homogeneous routes and even more so on microporous silicates (Table 2). Adsorption and confinement and their enthalpic stabilization of transition states also decrease their entropies, leading to activation entropies that are also more negative on mesoporous silica and zeolites than for homogeneous routes (Table 2). In particular, the negative activation energies, evident from the upward sloping lines in Figures 1 and 2, reflect transition states that are enthalpically more stable than the gaseous reactants. In the case

**Table 2. Measured Activation Enthalpies and Entropies for NO Oxidation in the Homogeneous Gas Phase and on Silica, SIL-1, SIL-1D, BEA, and CHA Zeolites Measured in the Range 278–373 K<sup>a</sup>**

	$\Delta H_{\text{eff}}^{\circ}$ [kJ mol <sup>-1</sup> ]	$\Delta S_{\text{eff}}^{\circ}$ [J mol <sup>-1</sup> K <sup>-1</sup> ]	$K_{\text{eff}}$ (325.5 K) [(mol m <sup>-3</sup> ) <sup>-2</sup> ] <sup>b</sup>
homogeneous reaction	-3.9 ± 0.7	-262.3 ± 2.2	8.40 × 10 <sup>-14</sup>
silica	-31.0 ± 4.6	-306.4 ± 14.3	9.32 × 10 <sup>-12</sup>
BEA	-35.8 ± 2.1	-295.6 ± 6.8	1.80 × 10 <sup>-10</sup>
SIL-1D	-39.5 ± 0.8	-296.3 ± 2.4	7.27 × 10 <sup>-10</sup>
SIL-1	-37.5 ± 12.4	-290.4 ± 37.3	7.06 × 10 <sup>-10</sup>
CHA	-41.2 ± 1.4	-309.2 ± 4.2	2.89 × 10 <sup>-10</sup>

<sup>a</sup>The equilibrium constants  $K_{\text{eff}}$  at 325.5 K are also shown for comparison. <sup>b</sup> $K_{\text{eff}}$  was obtained from activation free energies and is defined by:

$$K_{\text{eff}} = \frac{[\text{N}_2\text{O}_4]^{\ddagger}}{[\text{NO}]^2 [\text{O}_2]} = \left[\frac{\text{mol}}{m_{\text{ref}}^3}\right] \left[\frac{\text{mol}}{m_{\text{homog}}^3}\right]^{-3}$$

of the unconfined transition states that mediate homogeneous routes, the small negative enthalpy (-3.9 kJ mol<sup>-1</sup>) reflects the incipient formation of chemical bonds and the concomitant electrostatic stabilization via induced dipoles as an O<sub>2</sub> molecule and two NO molecules (the latter with radical character) reach interaction distances.

The observed enthalpy differences (Table 2) correspond to the enthalpy of confinement of the homogeneous transition state, including any enthalpy changes caused by the rearrangement of its constituent atoms as a result of confinement. These enthalpies resemble those for the confinement of small alkanes within purely siliceous micropores.<sup>36–40</sup> The volume of N<sub>2</sub>O<sub>4</sub>, used as a proxy for the transition state, is 0.106 nm<sup>3</sup>, while those for ethane and propane are 0.091 nm<sup>3</sup> and 0.148 nm<sup>3</sup>, respectively (from their liquid densities). On SIL-1, adsorption enthalpies were -32 kJ mol<sup>-1</sup> for ethane, -42 kJ mol<sup>-1</sup> for propane<sup>40</sup> (276–354 K) at low coverage, and on H-ZSM-5 -41 kJ mol<sup>-1</sup> for propane and -52 kJ mol<sup>-1</sup> for *n*-butane,<sup>41</sup> similar to the confinement enthalpies of the NO oxidation transition state on siliceous zeolites (SIL-1 -33.6 and SIL-1D -35.6 kJ mol<sup>-1</sup>; Table 3). Transition state confinement

**Table 3. Differences in Enthalpy and Entropy between the Transition States (N<sub>2</sub>O<sub>4</sub><sup>‡</sup>) for Catalytic and Homogeneous NO Oxidation Routes**

catalyst	$\Delta H_{\text{cat}}^{\circ\dagger} - \Delta H_{\text{homog}}^{\circ\dagger}$ [kJ mol <sup>-1</sup> ]	$\Delta S_{\text{cat}}^{\circ\dagger} - \Delta S_{\text{homog}}^{\circ\dagger}$ [J mol <sup>-1</sup> K <sup>-1</sup> ]
silica	-27.1 ± 4.7	-41.5 ± 14.5
BEA	-31.9 ± 2.2	-33.3 ± 7.1
SIL-1D	-35.6 ± 1.1	-34.0 ± 3.3
SIL-1	-33.6 ± 12.4	-28.1 ± 37.4
CHA	-37.3 ± 1.6	-46.9 ± 4.7

enthalpies become more negative as voids become smaller, as is also the case for small alkanes,<sup>41</sup> because smaller voids provide more effective van der Waals contacts with the N<sub>2</sub>O<sub>4</sub><sup>‡</sup> species that mediate NO oxidation.

The loss of entropy upon confinement of NO oxidation transition states is also reminiscent of the loss of degrees of freedom that accompanies the confinement of small molecules within zeolite voids. Activation entropies are large and negative even for unconfined transition states in homogeneous NO

oxidation ( $-262.3 \text{ J mol}^{-1} \text{ K}^{-1}$ ), because of their termolecular stoichiometry. Adsorption on mesoporous silica or confinement within zeolite voids by the transition state leads to an additional entropy loss (from  $-33$  to  $-47 \text{ J mol}^{-1} \text{ K}^{-1}$ , Table 2) because translational modes become frustrated within voids of molecular size. The entropy of confinement of propane on SIL-1 is  $-90 \text{ J mol}^{-1} \text{ K}^{-1}$ .<sup>42</sup> These values are significantly more negative than for confinement of the NO oxidation transition state within microporous solids ( $-47$  to  $-33 \text{ J mol}^{-1} \text{ K}^{-1}$ ); such differences reflects the additional vibrational and rotational modes in gaseous alkanes compared with  $\text{N}_2\text{O}_4$ -like transition states, which become frustrated upon confinement, causing their entropy losses upon confinement to be much larger than those for NO oxidation transition states.

The catalytic consequences of confinement reflect changes in the enthalpy and entropy of the transition state as a result of placing such species near surfaces and within voids of molecular dimensions, where intramolecular interactions occur in concert with van der Waals interactions with framework oxygens on silicate surfaces. Enthalpic stabilization by confinement or adsorption causes concomitant losses in entropy. As a result, confinement leads to rate enhancements only when such compensation effects decrease Gibbs free energies for transition states, which determine the dynamics of chemical transformations in the context of transition state theory. The functional form of the defining equation for the Gibbs free energy

$$\Delta G = \Delta H - T\Delta S \quad (18)$$

shows that the entropy losses that accompany enthalpic stabilization by confinement or adsorption become less consequential at low temperatures,<sup>43</sup> causing enthalpic stabilization, specifically here for NO oxidation at near ambient temperatures, to prevail and to lead to the remarkable rate enhancements observed. NO oxidation at near ambient temperatures serves as a striking example of physical catalysis, which cause chemical transformations to occur at faster rates merely as a consequence of nonspecific van der Waals interactions, which stabilize the relevant transition state without requiring specific binding to a catalytically active site.

## 5. CONCLUSIONS

We have demonstrated that high surface area silicas and crystalline microporous zeolites (MFI, CHA and BEA) are all effective catalysts for the oxidation of NO by dioxygen to form  $\text{NO}_2$  in the temperature range 278–435 K, despite the absence of a well-defined active site for the binding of reactants and products. The observed NO oxidation rates are much higher (by factors of  $10^4$ ) than homogeneous reaction rates. The measurements show reaction orders of 1 and 2 in NO and  $\text{O}_2$ , respectively, that are the same observed for the gas-phase homogeneous NO oxidation. This indicates that NO oxidation reaction proceeds via elementary steps reminiscent of those in homogeneous reactions, but with selective stabilization of the relevant termolecular transition states via physical confinement. Areal reaction rates are higher on the microporous materials than on the amorphous silica under all the conditions investigated (278–435 K). The apparent activation energy is negative in all cases. The precise structure of transition states, as well as the details of the reaction paths that lead to the formation of the transition states, are not accessible through the kinetic measurements reported herein. Nonetheless, the measured rate constants, that relate the kinetically relevant

transition state to the gas phase reactants, can be analyzed within the framework of the transition state theory. This yields negative enthalpies of formation of the transition states ( $-31$  to  $-41.2 \text{ kJ mol}^{-1}$ ) as well as negative entropies of formation ( $-262.3$  to  $-309.2 \text{ J mol}^{-1} \text{ K}^{-1}$ ) with respect to the gas phase reactants.

Such values show that the observed catalytic reaction rates are due to the enthalpic stabilization of the transition states that more than compensates for the kinetic costs of the negative entropy of formation of the transition states within the materials' micropores.

## ■ ASSOCIATED CONTENT

### Supporting Information

Appendix: Estimation of activation enthalpies and entropies of the transition states ( $\text{N}_2\text{O}_4^\ddagger$ ) for catalytic and homogeneous NO oxidation routes. This material is available free of charge via the Internet at <http://pubs.acs.org>.

## ■ AUTHOR INFORMATION

### Present Addresses

<sup>†</sup>N.A.: Laboratory of Catalysis and Catalytic Processes, Energy Department, Politecnico di Milano - p.za Leonardo da Vinci, 32 - 20133 Milan, Italy.

<sup>‡</sup>R.F.L.: Center for Catalytic Science and Technology, Department of Chemical and Biomolecular Engineering, University of Delaware, Newark, Delaware 19716, United States (permanent address).

### Notes

The authors declare no competing financial interest.

## ■ ACKNOWLEDGMENTS

We acknowledge with thanks the financial support from the Chemical Sciences Division, Office of Basic Energy Sciences, Office of Science, U.S. Department of Energy under grant number DE-FG02-03ER15479 is also gratefully acknowledged. We also acknowledge Professor Rajamani Gounder of Purdue University for technical suggestions and his careful proof-reading of the manuscript.

## ■ REFERENCES

- (1) Monks, P. S. Gas-phase radical chemistry in the troposphere. *Chem. Soc. Rev.* **2005**, *34*, 376–395.
- (2) Tsukahara, H.; Ishida, T.; Mayumi, M. Gas-phase oxidation of nitric oxide: Chemical kinetics and rate constant. *Nitric Oxide* **1999**, *3* (3), 191–198.
- (3) Bodenstein, M.; Wachenheim, L. Die Geschwindigkeit der Reaktion zwischen Stickoxyd und Sauerstoff. *Z. Elektrochem.* **1918**, *24*, 183–201.
- (4) Mulla, S. S.; Chena, N.; Cumarantunge, L.; Blau, G. E.; Zemlyanov, D. Y.; Delgass, W. N.; Epling, W. S.; Ribeiro, F. H. Reaction of NO and  $\text{O}_2$  to  $\text{NO}_2$  on Pt: Kinetics and catalyst deactivation. *J. Catal.* **2006**, *241*, 389–399.
- (5) Hisatsun, I.; Zafonte, L. A kinetic study of some third-order reactions of nitric oxide. *J. Phys. Chem.* **1969**, *73* (9), 2980–2989.
- (6) (a) Beckers, H.; Zeng, X. Q.; Willner, H. Intermediates Involved in the Oxidation of Nitrogen Monoxide: Photochemistry of the *cis*- $\text{N}_2\text{O}_2\text{-O}_2$  complex and of *sym*- $\text{N}_2\text{O}_4$  in Solid Ne Matrices. *Chem.—Eur. J.* **2010**, *16* (5), 1506–1520. (b) Gadzhiev, O. B.; Ignatov, S. K.; Razuvaev, A. G.; Masunov, A. E. Quantum Chemical Study of Trimolecular Reaction Mechanism between Nitric Oxide and Oxygen in the Gas Phase. *J. Phys. Chem. A* **2009**, *113* (32), 9092–9101.
- (7) (a) Fickel, D. W.; D'Addio, E.; Lauterbach, J. A.; Lobo, R. F. The ammonia selective catalytic reduction activity of copper-exchanged

- small-pore zeolites. *Appl. Catal., B* **2011**, *102* (3–4), 441–448.
- (b) Delahay, G.; Valade, D.; Guzman-Vargas, A.; Coq, B. Selective catalytic reduction of nitric oxide with ammonia on Fe-ZSM-5 catalysts prepared by different methods. *Appl. Catal., B* **2005**, *55* (2), 149–155.
- (8) Luo, J. Y.; Hou, X.; Wijayakoon, P.; Schmiege, S. J.; Li, W.; Epling, W. S. Spatially resolving SCR reactions over a Fe/zeolite catalyst. *Appl. Catal., B* **2011**, *102*, 110–119.
- (9) Brandenberger, S.; Kröcher, O.; Tissler, A.; Althoff, R. The State of the Art in Selective Catalytic Reduction of NO<sub>x</sub> by Ammonia Using Metal Exchanged Zeolite Catalysts. *Catal. Rev.: Sci. Eng.* **2008**, *50*, 492–531.
- (10) Metkar, P. S.; Balakotaiah, V.; Harold, M. P. Experimental and kinetic modeling study of NO oxidation: Comparison of Fe and Cu-zeolite catalysts. *Catal. Today* **2012**, *184*, 115–128.
- (11) Shwana, S.; Jansson, J.; Korsgren, J.; Olsson, L.; Skoglundh, M. Kinetic modeling of H-BEA and Fe-BEA as NH<sub>3</sub>-SCR catalysts—Effect of hydrothermal treatment. *Catal. Today* **2012**, *197*, 24–37.
- (12) (a) Brandenberger, S.; Krocher, O.; Tissler, A.; Althoff, R. The State of the Art in Selective Catalytic Reduction of NO<sub>x</sub> by Ammonia Using Metal-Exchanged Zeolite Catalysts. *Catal. Rev.: Sci. Eng.* **2008**, *50* (4), 492–531. (b) Szanyi, J.; Paffett, M. T. The adsorption of NO and reaction of NO with O<sub>2</sub> on H-, NaH-, CuH-, and Cu-ZSM-5: An in situ FTIR investigation. *J. Catal.* **1996**, *164* (1), 232–245. (c) Despres, J.; Koebel, M.; Krocher, O.; Elsener, M.; Wokaun, A. Storage of NO<sub>2</sub> on BaO/TiO<sub>2</sub> and the influence of NO. *Appl. Catal., B* **2003**, *43* (4), 389–395.
- (13) Xu, L.; McCabe, R. W. LNT + in situ SCR catalyst system for diesel emissions control. *Catal. Today* **2012**, *184*, 83–94.
- (14) Jen, H.-W.; Graham, G. W. Promotion of the NO+O<sub>2</sub> reaction by Ba–Y, FAU zeolite at 25 °C. *Catal. Lett.* **2006**, *108*, 21–23.
- (15) Halasz, I. B., A.; Ng, K. Y. S. Active sites of H-ZSM5 catalysts for the oxidation of nitric oxide by oxygen. *Catal. Lett.* **1995**, *34* (1–2), 151–161.
- (16) Richter, M.; Eckelt, R.; Parlitz, B.; Fricke, R. Low-temperature conversion of NO<sub>x</sub> to N<sub>2</sub> by zeolite-fixed ammonium ions. *Appl. Catal. B* **1998**, *15* (1–2), 129–146.
- (17) (a) Szanyi, J.; Kwak, J. H.; Moline, R. A.; Peden, C. H. F. The adsorption of NO<sub>2</sub> and the NO+O<sub>2</sub> reaction on Na-Y,FAU: an in situ FTIR investigation. *Phys. Chem. Chem. Phys.* **2003**, *5* (18), 4045–4051. (b) Szanyi, J.; Kwak, J. H.; Peden, C. H. F. The effect of water on the adsorption of NO<sub>2</sub> in Na- and Ba-Y, FAU zeolites: A combined FTIR and TPD investigation. *J. Phys. Chem. B* **2004**, *108* (12), 3746–3753. (c) Hadjiivanov, K.; Penkova, A.; Daturi, M.; Saussey, J.; Lavalley, J. C. FTIR spectroscopic study of low-temperature co-adsorption of NO and O<sub>2</sub> on H-ZSM-5: evidence of formation of ONNO (+) species. *Chem. Phys. Lett.* **2003**, *377* (5–6), 642–646. (d) Hadjiivanov, K.; Saussey, J.; Freysz, J. L.; Lavalley, J. C. FT-IR study of NO+O<sub>2</sub> co-adsorption on H-ZSM-5: re-assignment of the 2133 cm<sup>-1</sup> band to NO<sup>+</sup> species. *Catal. Lett.* **1998**, *52* (1–2), 103–108.
- (18) Derouane, E. G. Zeolites as solid solvents. *J. Mol. Catal. A: Chem.* **1998**, *134*, 29–45.
- (19) Caillet, P.; Paillaud, J. L.; Simon-Masseron, A.; Souillard, M. P., J. The fluoride route: a strategy to crystalline porous materials. *C. R. Chim.* **2005**, *8* (3–4), 245–266.
- (20) (a) Bordiga, S.; Roggero, I.; Ugliengo, P.; Zecchina, A., B. V.; Artioli, G.; Buzzoni, R.; Marra, G. L.; Rivetti, F.; Spano, G.; Lamberti, C. Characterization of defective silica. *J. Chem. Soc., Dalton Trans.* **2000**, *21*, 3921–3929. (b) Koller, H.; Lobo, R. F.; Burkett, S. L.; Davis, M. E. SiO<sup>-</sup>...HOSi Hydrogen-Bonds in as-Synthesized High-Silica Zeolites. *J. Phys. Chem.* **1995**, *99* (33), 12588–12596.
- (21) Fickel, D. W.; Shough, A. M.; Doren, D. J.; Lobo, R. F. High-temperature dehydrogenation of defective silicalites. *Microporous Mesoporous Mater.* **2010**, *129* (1–2), 156–163.
- (22) Pinar, A. B.; Hould, N.; Lobo, R. F., unpublished results.
- (23) Eilertsen, E. A.; Arstad, B.; Svete, S.; Lillerud, K. P. Single parameter synthesis of high silica CHA zeolites from fluoride media. *Microporous Mesoporous Mater.* **2012**, *153*, 94–99.
- (24) Rouquerol, J.; Rouquerol, F.; Sing, K. S. W. *Adsorption by powders and porous solids: Principles, Methodology and Applications*, 1st ed.; Academic Press: London, 1999.
- (25) Webb, P. A.; Orr, C. *Analytical Methods in Fine Particle Technology*; Micromeritics Instrument Corp.: Norcross, GA, 1997.
- (26) Diaz-Cabanias, M. B., PA; Cambor, M. A. Synthesis and structure of pure SiO<sub>2</sub> chabazite: the SiO<sub>2</sub> polymorph with the lowest framework density. *Chem. Commun.* **1998**, No. 17, 1881–1882.
- (27) Groen, J. C.; Abello, S. V., L. A.; Perez-Ramírez, J. Mesoporous beta zeolite obtained by desilication. *Microporous Mesoporous Mater.* **2008**, *114*, 93–102.
- (28) Cambor, M. A.; Valencia, A. C., S. Characterization of nanocrystalline zeolite Beta. *Microporous Mesoporous Mater.* **1998**, *25* (1–3), 59–74.
- (29) Trzpit, M. S.; Patarin, J.; Desbiens, N.; Cailliez, F.; Boutin, A.; Demachy, I.; Fuchs, A.H. The effect of local defects on water adsorption in silicalite-1 zeolite: A joint experimental and molecular simulation study. *Langmuir* **2007**, *23*, 10131–10139.
- (30) <http://www.iza-structure.org/databases/>.
- (31) (a) Glasson, W. A.; Tuesday, C. S. The atmospheric thermal oxidation of nitric oxide. *J. Am. Chem. Soc.* **1963**, *85*, 2901–2904. (b) Hasche, R. L.; Patrick, W. A. Studies on the rate of oxidation of nitric oxide. II. The velocity of the reaction between nitric oxide and oxygen at 0° and 30°. *J. Am. Chem. Soc.* **1925**, *47*, 1207–1215.
- (32) Olbregts, J. Termolecular reaction of nitrogen mon- oxide and oxygen: A still unsolved problem. *Int. J. Chem. Kinet.* **1985**, *17*, 835–848.
- (33) Galliker, B.; Kissner, R.; Nauser, T.; Koppenol, W. H. Intermediates in the Autoxidation of Nitrogen Monoxide. *Chem.—Eur. J.* **2009**, *15* (25), 6161–6168.
- (34) Perry, R. H.; Green, D. *Perry's Chemical Engineers Handbook*, 6th ed.; McGraw-Hill: New York, 1984.
- (35) Robinson, P. J. Dimensions and Standard States in the Activated Complex Theory of Reaction Rates. *J. Chem. Educ.* **1978**, *55* (8), 509–510.
- (36) Eder, F. L., J. A. Alkane Sorption on Siliceous and Aluminophosphate Molecular Sieves. A Comparative Study. *J. Phys. Chem.* **1996**, *100*, 16460–16462.
- (37) Eder, F.; Lercher, J. A. Alkane sorption in molecular sieves: The contribution of ordering, intermolecular interactions, and sorption on Bronsted acid sites. *Zeolites* **1997**, *18*, 75–81.
- (38) Janchen, J.; Stach, H.; Uytterhoeven, L.; Mortier, W. J. Influence of the Framework Density and the Effective Electronegativity of Silica and Aluminophosphate Molecular Sieves on the Heat of Adsorption of Nonpolar Molecules. *J. Phys. Chem.* **1996**, *100*, 12489–12493.
- (39) McCullen, S. B.; Reischmann, P. T.; Olson, D. H. Influence of the Framework Density and the Effective Electronegativity of Silica and Aluminophosphate Molecular Sieves on the Heat of Adsorption of Nonpolar Molecules. *Zeolites* **1993**, *13*, 640–644.
- (40) Sun, M. S.; Shah, D. B.; Xu, H. H.; Talu, O. Adsorption Equilibria of C1 to C4 Alkanes, CO<sub>2</sub>, and SF<sub>6</sub> on Silicalite. *J. Phys. Chem. B* **1998**, *102*, 1466–1473.
- (41) De Moor, B. A.; Reyniers, M. F.; Gobin, O. C.; Lercher, J. A.; Marin, G. B. Adsorption of C<sub>2</sub>-C<sub>8</sub> n-Alkanes in Zeolites. *J. Phys. Chem. C* **2011**, *115*, 1204–1219.
- (42) Zhu, W.; Kapteijn, F.; Mouleijn, J. Equilibrium Adsorption of Light Alkanes in Silicalite-1 by the Inertial Microbalance Technique. *Adsorption* **2000**, *6*, 159–167.
- (43) Gounder, R.; Iglesia, E. The Catalytic Diversity of Zeolites: Confinement and Solvation Effects within Voids of Molecular Dimensions. *Chem. Commun.* **2013**, *49*, 3491–3509.